Clutter Detection and Surface/Subsurface Slope Determination by Combination of Repeat-Pass Sounder Orbits Applied to SHARAD Data

Maria Carmela Raguso, Marco Mastrogiuseppe, and Roberto Seu

***Abstract*— Nadir-looking low-frequency radar sounders cannot easily resolve off-nadir surface returns from the subsurface nadir echoes. Cross-track surface echoes (also named "clutter") with time delays synchronized with subsurface returns are renowned for being a major challenge for scientists, as they can affect the analysis of orbital radar sounders data. We present a method for clutter discrimination and surface/subsurface slope estimation using data acquired from radar sounders in closely spaced repeated orbits configuration. The method takes advantage of cross-track signal migration to discriminate off-nadir clutter from subsurface signal returns received at the nadir. The migration of the off-nadir signals is also used to determine the clutter direction of arrival (DOA) as well as the surface/subsurface cross-track slopes. The effectiveness of the method has been proven on the Mars Reconnaissance Orbiter (MRO)'s Shallow Radar (SHARAD) dataset and provides a proof-of-concept demonstration for the surface clutter discrimination when radar sounders repeated-passes data are available.**

***Index Terms*— Clutter, ground penetrating radar, Mars, planetary radar, repeat pass.**

I. Introduction

THE use of radars for subsurface investigation is a well-known technique exploited for decades on Earth and planetary exploration [1], [2], [3]. For achieving penetration capabilities, radar sounders are usually designed to operate at long wavelengths [i.e., 1–40 MHz; HF/very high frequency (VHF) bands] that require the use of dipole antennas with low directivity. As a result, returns from off-nadir directions can mask subsurface signals of interest or, in the worst case, lead to an ambiguity that compromises the interpretation of subsurface features, especially when a single sounder or single-channel radar is employed. Typically, cross-track clutter discrimination is performed by visual [4], [5] or automatic [6] comparison between sounder data products ("radargram", RDR) and simulated products ("cluttergram") obtained using digital elevation models (DEMs) of the surface. However, this approach enables clutter identification only when the off-nadir clutter is exposed, and surface topography is available at a better scale than the radar ground resolution. First attempt to discriminate clutter without employing DEMs has been proposed in [7]. By comparing radargrams, the technique allows to profile the topographic variations and discriminate subsurface structure from off-nadir artifacts. Only recently, clutter detection techniques have been also proposed for multiaperture antenna sounders [8]; distributed radar sounding systems [9], [10]; or sounder repeat passes [11].

Herein, starting from the MOC assumptions [7], we address this critical problem by proposing a technique for surface clutter discrimination as well as the estimation of surface/subsurface slopes in orbital sounder data. By incoherently combing radar sounders data acquired at different epochs in adjacent-orbit configurations and by taking advantage of the clutter cross-track migration in the radar products, the proposed method allows not only the clutter discrimination but also solves the left/right clutter ambiguity. In this way, the proposed technique aims to generate new sounder products by fusing two (or more) single-pass sounder observations. The new two-color final product (or stereo image) represents a fast and easy visual way for scientists to study radargrams. It allows to derive more robust interpretations and discriminate between actual and false subsurface features due to the clutter, wherever a pair (or more) of adjacent sounding tracks in a suitable configuration is available. This technique will certainly facilitate the radar sounders data interpretation and further enhance the clutter discrimination performances with respect to traditional single-pass radar sounder techniques. The proposed method not only enables the identification of clutter returns not detectable via simulations, but it also has the ability to efficiently resolve the inherent clutter direction-of-arrival (DOA) ambiguities and detect surface/subsurface slopes (i.e., discrete clutter returns from the subsurface). Solving these last two aspects is a nontrivial problem, as they can severely compromise the sounders data interpretation, and their effects are not easily untangled from the nadir returns especially when a single-pass sounder is employed. The approach developed in this letter has wide applicability and can be considered a

Manuscript received 5 May 2022; revised 27 July 2022 and 31 October 2022; accepted 17 November 2022. Date of publication 21 November 2022; date of current version 6 December 2022. This work was supported by the Jet Propulsion Laboratory, California Institute of Technology, Pasadena, CA, USA, within the National Aeronautics and Space Administration, under Contract 80NM0018D0004. *(Corresponding author: Maria Carmela Raguso.)*

Maria Carmela Raguso was with the Dipartimento di Ingegneria dell'Informazione, Elettronica e Telecomunicazioni (DIET), Sapienza Università di Roma, 00184 Rome, Italy. She is now with the Jet Propulsion Laboratory, California Institute of Technology, Pasadena, CA 91125 USA (e-mail: maria.raguso@jpl.nasa.gov).

Marco Mastrogiuseppe and Roberto Seu are with the Dipartimento di Ingegneria dell'Informazione, Elettronica e Telecomunicazioni (DIET), Sapienza Università di Roma, 00184 Rome, Italy (e-mail: marco.mastrogiuseppe@uniroma1.it; roberto.seu@uniroma1.it).

Digital Object Identifier 10.1109/LGRS.2022.3223882

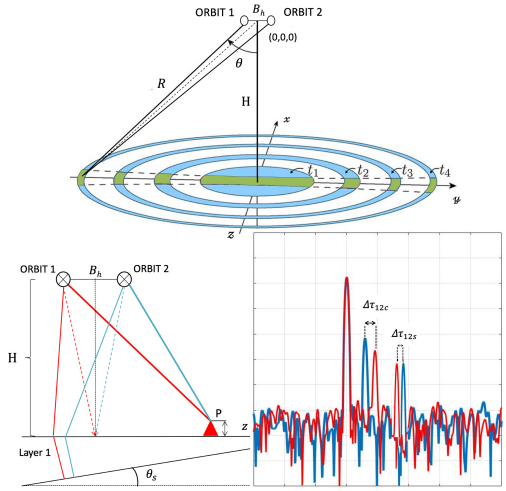

Fig. 1. (Top) Repeated-pass geometry. Orbit1 and Orbit2 correspond to the two positions of the orbiter at height H above the surface and separated by a horizontal baseline B_h. Annuli in blue represent ground resolution cells at different time instants (and in green the corresponding pulse limited resolution cells after Doppler processing). (Bottom left) Cross-track clutter and subsurface slope discrimination. Nadir returns (red/cyan dashed lines) are received synchronous from the surface, while cross-track clutter and Layer1 returns (red/cyan solid lines) are delayed of $\Delta\tau_{12c}$ and $\Delta\tau_{12s}$, respectively, according to the geometry. (Bottom right) Simulated radar waveforms as received by Orbit1 (red) and Orbit2 (cyan).

stand-alone alternative to the clutter simulators when dense coverage and orbital configuration requirements are satisfied (i.e., near-circular orbits).

II. Method for Cross-Track Clutter Discrimination and Slope Estimation

Assuming a nadir-looking sensor, the clutter footprints corresponding to different depths of ambiguity are described by annuli, as illustrated in Fig. 1. After doppler focusing, the clutter problem reduces to the across-track direction in the form of surface returns from angles $\pm\theta$. The proposed method takes advantage of the cross-track clutter migration observed over closely spaced radar adjacent tracks to discriminate the nadir return (no migration) from off-nadir clutter returns (migration as a function of the angle). Depending on the orbital geometry of the radar acquisitions, the effects of this migration can be more or less pronounced. Large horizontal baselines (see B_h in Fig. 1) are favorable for the proposed method, since clutter migration is amplified. On the other hand, small baselines preserve correlation but reduce the cross-track migration, making the clutter discrimination impracticable at shallow depths. Therefore, we can define an optimal interval for B_h where the upper limit ($B_{\max}$) is chosen to be 50% of footprint overlapping, while the lower limit ($B_{\min}$) is equal to the full migration of the first range cell projected onto the terrain. For a pulse limited system, we can define the cross-track ground projected as follows:

$$R_{yi} = \sqrt{2H\delta} \cdot \left(\sqrt{i} - \sqrt{i-1}\right) \tag{1}$$

where H is the spacecraft altitude, δ is the radar range resolution, and i is the annulus number [i.e., $i = 1$ for the pulse limited radius, and $i = 2$ for the first annulus see Fig. 1)]. It follows that the optimal values for B_h are within $B_{\min} = 0.41 \cdot (2H\delta)^{1/2}$ and $B_{\max} = (2H\delta)^{1/2}$. For the case

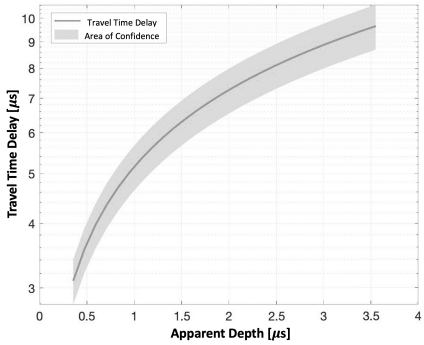

Fig. 2. Theoretical relationship between the travel time delay ($\Delta\tau_{12c}$) and the apparent depth converted in time ($\Delta\tau_1$) for a scenario with $B_h = 800$ m, $H = 285$ km, and considering a clutter with a variable elevation of about ± 150 m (area of confidence). Note that, if the time shift of the detected off-nadir signals ($\Delta\tau_{12c}$) belongs to the curve, the clutter is more likely originated by the surface topography, otherwise from subsurface slope or volume clutter.

of Shallow Radar (SHARAD), we obtain $B_{\min} \cong 850$ m and $B_{\max} = 3$ km. Note that for lower values of $B_{\min}$, the method is still applicable, but its sensitivity decreases due to the moderate migration effects. For values greater than $B_{\max}$ instead, the decorrelation between products increases, making the co-registration process challenging. Let us define the time delays of an off-nadir clutter received at the two antennas locations as $\Delta\tau_{1c}$ and $\Delta\tau_{2c}$; by measuring their difference ($\Delta\tau_{12c}$), an estimation of the clutter angle of arrival can be performed. The time delay measured from clutter migration can be converted into angle of arrival using the following:

$$\theta = \tan^{-1}\left(B_p/B_h\right) \tag{2}$$

where B_p is the parallel baseline described as follows:

$$B_p = \Delta\tau_{12c} \cdot c/2 \tag{3}$$

with c is the speed of light. Using the same multiorbit approach, also, surface local slopes can be treated similar to the clutter and estimated using (2). When in addition to the surface, a sloped subsurface reflector is present (see the case of $\Delta\tau_{12s}$ in Fig. 1), the difference in travel time between the returns at the two adjacent orbits ($\Delta\tau_{12s} = \Delta\tau_{1s} - \Delta\tau_{2s}$) is purely function of the local slope of the layer θ_s and can be estimated as in [12] by the following formula:

$$\Delta\tau_{12s} = 2 * B_h * \frac{\tan(\theta_s)}{c * n * \cos(\theta_s)}. \tag{4}$$

Note that returns due to the clutter will have a predictable time delay ($\Delta\tau_{12s}$) for a given apparent depth $\Delta\tau_1$ explicable with the theoretical curve in Fig. 2. In this way, the interpretational ambiguity between sloped subsurface and lateral clutter can be addressed.

III. Co-Registration and Overlaying of Images

As previously mentioned, the general idea behind the proposed method is to produce a stereo image by combining pairs of radargrams acquired by the same sensor in repeat-pass configuration. The new image improves the clutter detection with the additional capability to solve the inherent clutter DOA ambiguities that characterize the sounding data. A co-registration step between radargrams is a key requirement before overlaying the two radar observations.

Co-registration is performed in two steps, and it aims to correct all the geometric distortions between the radar products due to external factors (e.g., different ionospheric delays [13] and acquisition geometries). First, a cross correlation between the detected power profiles is performed in along-track to compensate azimuth misalignment. Note that the standard SHARAD data products do not address speckle noise (e.g., using "multilooks"), so we reduced speckle effects in the RDRs by smoothing the surface power profiles by a factor of 5 in order to mitigate the variability due to the speckle and limiting the speckle decorrelation effects. Once the two products are aligned in azimuth, a fine registration in time (or range domain) is performed using the offset center of gravity (OCOG) tracker [14]. Due to the large baselines involved, radar products are only partially correlated; hence, the OCOG has been preferred to the classical cross-correlation techniques. Unlike nadir returns, surface clutter returns at large angles (and thus large delays) turn out to be very decorrelated in products acquired in parallel configuration. This would result in co-registration problems if the overall received waveform is considered in the tracking process. The OCOG algorithm, instead of the threshold retracking, tends to track only the nadir returns that are less affected by the signal migration, making the co-registration step more robust. The two power profiles obtained by applying the OCOG tracker to each observation separately are then subtracted in order to calculate the time delay between the two observations due to geometrical or ionospheric distortions. The most probable value (i.e., the mode value) of the estimated time difference vector is then used to infer the time shift we use to compensate for the delay between the two radargrams. Assuming that the effects of the ionosphere are negligible (or constant) within each track, the estimated time delay between the two parallel observations is, thus, a constant value along the entire track, and it can be used for compensating the misalignment between the two radargrams. In contrast, in the case that nonstationary ionospheric conditions characterize the observations, the time delay is estimated using a polynomial fitting applied to the OCOG tracker. Since each SHARAD data product is an aggregation of SHARAD data blocks (SHARAD SCET block) collected continuously using the same operation mode, instrument status, and on-board processing scheme, we assume the ionosphere spatial variations to be lower than the topographic ones, and thus, a low-order polynomial (i.e., third or fourth order) is applied to each SHARAD SCET block to compensate for any possible misalignment due to the processing. After the co-registration process, the two radar products are overlaid to generate false-color compositions [i.e., cyan–red (CR)] that allow a fast and easy interpretation of features by means of a color code. According to this color code, the new product shows the nadir surface and eventually subsurface returns in bright white pixels, while cyan and red pixels are associated with returns that migrates in the two radargrams and, thus, associated with the off-nadir returns. In addition, from the order of the color sequence (i.e., cyan/red or red/cyan) and from their time delay, the new product enables clutter DOA estimation and solves the left/right ambiguity.

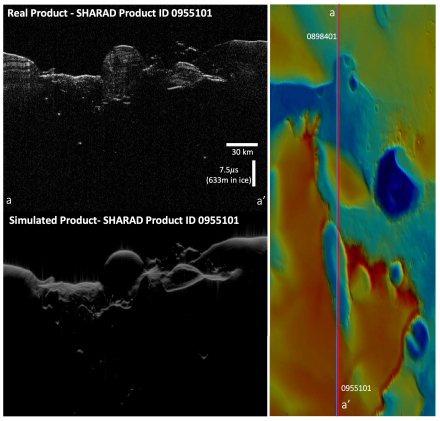

Fig. 3. (Top left) SHARAD real data. (Bottom Left) Simulated product. (Right) MOLA shaded relief at 128 ppd (≈460 m per pixel) map; letters a and a′ mark the position of one track (0898401; blue line) relative to the other (0955101; red line).

IV. Results

In this section, we present the results of the proposed tool applied to data collected by the SHARAD sounder. SHARAD is a 10-MHz wideband sounder, currently orbiting around Mars, on a subpolar (87.4° inclination) and near-circular orbit [2]. During 16 years of operations, SHARAD collected more than 30 000 observations, allowing a large coverage of Mars and several opportunities for repeated tracks. Note that, as a preprocessing step, we verified the absence of surface slopes using Mars Orbiter Laser Altimeter (MOLA) topographic data. Moreover, in both the cases of study, we neglect the ephemeris uncertainty, assuming that the only source of error in estimating the angle is due to the $\Delta\tau_{12c}$ uncertainness.

A. South Polar Layered Deposit

We present the results of the processing applied to a pair of observations collected over the Martian south polar layered deposit (SPLD) [15]. The two products have been acquired with a temporal baseline of 44 days and a horizontal baseline of 1.4 km. Fig. 3 shows one of the products available at the Planetary Data System (PDS) node. Here, subsurface returns appear interrupted and commingled with the off-nadir clutter returns, making sounder data interpretation challenging when using a single sounder product. Fig. 4 shows the stereo image obtained combining the two tracks. Subsurface reflections appear in bright white (see layers located between 81°S and 81.5°S), while off-nadir returns located at approximately −79.8°S appear in double color. DOA of the clutter can be easily identified from the stereo image because of the sequence of the colors. In our example, the sequence red/cyan for the clutter at 80.4°S (see Fig. 4—1) suggests that the DOA is East at an angle of about 5.1° ± 0.1°. Contrariwise, the clutter at 79.8°S shows the sequence cyan/red (see Fig. 4—2), meaning that the clutter is arriving from West at an angle of 4° ± 0.1°. We can convert the angle of arrival in across-track distance corresponding to ≈22.5 ± 0.5 and ≈17.7 ± 0.5 km, respectively. Fig. 4 (middle and bottom) shows the MOLA digital elevation model (MOLA-DEM) and the relative across-track profiles associated with our clutter returns. In both cases, the clutter sources can be identified on the topography

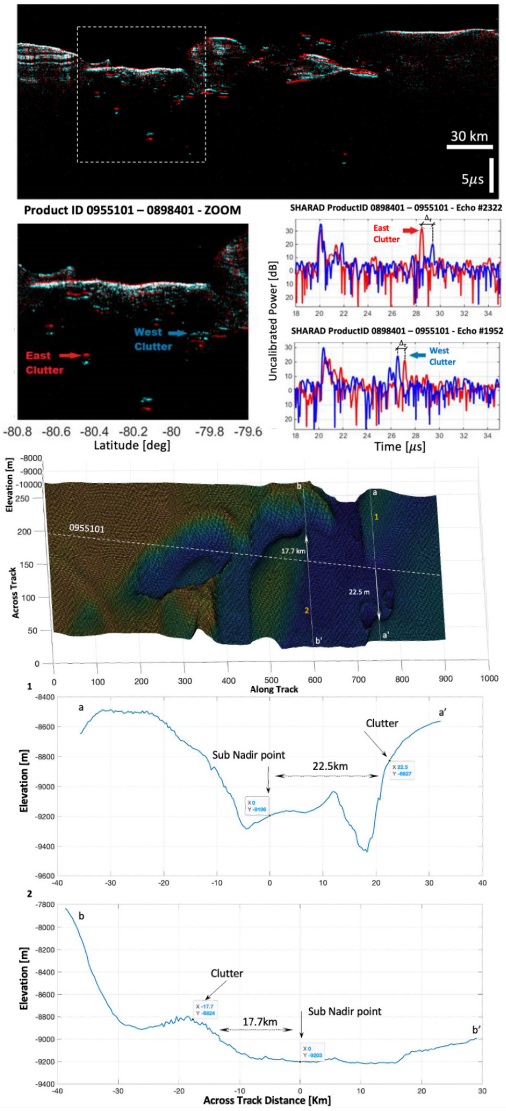

Fig. 4. (Top) Stereo image obtained by combining the two products and a zoomed-in view of the stereo image where West and East cross-track clutter returns are identified with colors and easily discriminated. Radar waveforms on the right allow to estimate the delay time difference of the clutter arrival (Δ_τ). (Middle) MOLA topographic DEM and radar ground track (white dashed line); the white arrow identifies the source of the clutter returns in correspondence of Echo#2322 and #1952. (Bottom) Cross-track topography at the locations of the clutters respect to the sub-nadiral point. The plots show confirmation the cross-track distances and the West/East DOAs as deducted from the analysis of the stereo product.

at across-track distances consistent with the ones previously estimated.

B. Lobate Debris Aprons

The lobate debris aprons (LDAs) are areas located at the mid-northern latitudes, where several layered near surface structures composed predominantly of water ice have been detected [16]. We select two tracks acquired with a 40-days temporal baseline and a horizontal baseline of 785 m. Fig. 5 shows one of the real products (top left) compared with its MOLA-based clutter gram (bottom left) generated with [4]. Fig. 6 shows the stereo image as a result of our processing. Echo#922 appears in bright white color suggesting to be generated by a nadiral feature. This interpretation is

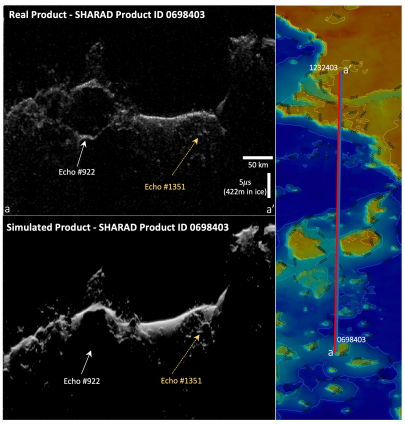

Fig. 5. (Top left) SHARAD real data. (Bottom left) Simulated product. White arrow points to a potential subsurface layer present in the real data but not in the simulated product (Echo#922), and yellow arrow points to several clutter returns due to the rough topography. (Right) MOLA map (128 ppd); letters a and a′ mark the position of one track (0698403; blue line) relative to the other (1232403; red line).

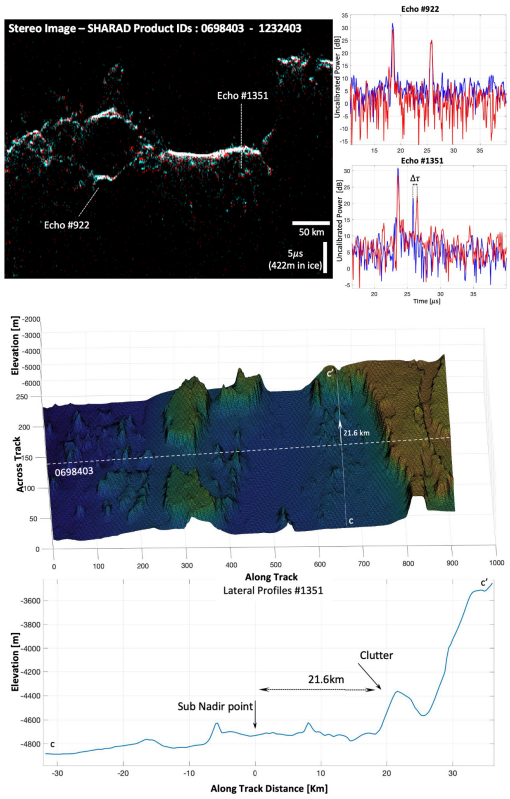

Fig. 6. (Top) Stereo image obtained with the proposed technique and relative radar waveforms of the detected subsurface return (Echo#922) and migrated clutter (Echo#1351). (Middle) MOLA topographic DEM and radar ground track (white dashed line); the white arrow identifies the source of the clutter returns in correspondence of Echo#1351. (Bottom) Cross-track topography at the location of the clutter. The estimated cross-track distance from nadir (i.e., 21.6 km) is consistent with the one measured from MOLA.

confirmed by the facet simulator that does not show any signal corresponding to that return, thus validating the subsurface hypothesis. On the other hand, Echo#1351 appears in double color, meaning that is produced by an off-nadir feature. By measuring the time delay between the clutter returns and using formula (3), we found a parallel baseline B_p of ≈62 m, suggesting that the angle of arrival is about 4.5° ± 0.2°.

The sequence of colors (i.e., cyan/red for the Echo#1351) allowed us also to identify that the clutter source comes from the East. This is consistent with the surface feature located at $\approx 21.6 \pm 0.8$-km East from the nadir track, as shown from the MOLA across-track profile in Fig. 6 (bottom).

V. Conclusion

We present a method to increase the cross-track clutter and the surface/subsurface slope discrimination and to improve the ability to detect subsurface layers when radar adjacent tracks are available. In cases when DEMs have no sufficient spatial resolution to properly represent features in the radargram, the proposed processing allows to discriminate clutter returns and drastically improve radar interpretation of the sounder radar products. The effectiveness of the approach has been proven on two datasets acquired by SHARAD. However, the proposed method has a general applicability and can be used to help scientists on radar data interpretation, for example, in the detection of subsurface water-ice resources at the Martian mid-latitudes [17] or looking ahead to the Jovian icy-moon sounders (radar for icy moon exploration (RIME) [18] and Radar for Europa Assessment and Sounding: Ocean to Near-Surface (REASON) [19]) in case geometrical orbital parameters allow repeated ground track to be acquired. Additional improvements to this clutter discrimination technique can be done by applying super-resolution techniques [20] to the radargrams before the co-registration step for improving the resolution of radar products. As future works, we plan to explore and test deep learning algorithms for automatic clutter features recognition [21] in orbital radar sounder products.

Acknowledgment

The authors would like to thank the Shallow Radar (SHARAD) Science Team, Italian Space Agency (ASI), Rome, Italy, and the SHARAD Operations Center (SHOC), Rome. They would also like to thank Veronica Russo for her support during her master thesis and Dr. D. C. Nunes for his comments that substantially improved this work.

References

[1] G. Picardi et al., "MARSIS: Mars advanced radar for subsurface and ionosphere sounding," *Mars Exp., Sci. Payload*, vol. 1240, pp. 51–69, Aug. 2004.

[2] R. Seu et al., "SHARAD sounding radar on the Mars reconnaissance orbiter," *J. Geophys. Res. Planets*, vol. 112, no. E5, pp. 1–18, 2007.

[3] T. Ono et al., "Instrumentation and observation target of the lunar radar sounder (LRS) experiment on-board the SELENE spacecraft," *Earth, planets space*, vol. 60, pp. 321–332, Sep. 2008.

[4] F. Russo et al., "An incoherent simulator for the SHARAD experiment," in *Proc. IEEE Radar Conf.*, May 2008, pp. 1–4.

[5] Y. Lei, M. C. Raguso, M. Mastrogiuseppe, C. Elachi, and M. S. Haynes, "Validation of a pseudospectral time-domain (PSTD) planetary radar sounding simulator with SHARAD radar sounding data," *IEEE Trans. Geosci. Remote Sens.*, vol. 60, pp. 1–15, 2022.

[6] A. Ferro, A. Pascal, and L. Bruzzone, "A novel technique for the automatic detection of surface clutter returns in radar sounder data," *IEEE Trans. Geosci. Remote Sens.*, vol. 51, no. 5, pp. 3037–3055, May 2013.

[7] W. J. Peeples et al., "Orbital radar evidence for lunar subsurface layering in Maria serenitatis and Crisium," *J. Geophys. Res., Solid Earth*, vol. 83, no. B7, pp. 3459–3468, Jul. 1978.

[8] D. Castelletti et al., "An interferometric approach to cross-track clutter detection in two-channel VHF radar sounders," *IEEE Trans. Geosci. Remote Sens.*, vol. 55, no. 11, pp. 6128–6140, Nov. 2017.

[9] M. S. Haynes et al., "Debris: Distributed element beamformer radar for ice and subsurface sounding," in *Proc. IEEE Int. Geosci. Remote Sens. Symp. (IGARSS)*, Jul. 2021, pp. 651–654.

[10] L. Carrer, S. Thakur, and L. Bruzzone, "Clutter discrimination by estimation of direction of arrival in spaceborne distributed radar sounders," in *Proc. IEEE Int. Geosci. Remote Sens. Symp. (IGARSS)*, Jul. 2022, pp. 1324–1327.

[11] M. Mastrogiuseppe, M. Raguso, R. Seu, and N. Putzig, "Surface clutter suppression using coherent processing of radar sounder data from repeated ground tracks," in *Proc. 50th Lunar Planet. Sci. Conf.*, no. 2132, 2019, p. 2967.

[12] D. Castelletti, D. M. Schroeder, E. Mantelli, and A. Hilger, "Unfocused SAR processing for englacial layer slope estimation using radar sounder data," in *Proc. IEEE Int. Geosci. Remote Sens. Symp.*, Jul. 2018, pp. 4150–4153.

[13] B. A. Campbell, N. E. Putzig, F. J. Foss, and R. J. Phillips, "SHARAD signal attenuation and delay offsets due to the Martian ionosphere," *IEEE Geosci. Remote Sens. Lett.*, vol. 11, no. 3, pp. 632–635, Mar. 2014.

[14] T. Bucciarelli, S. Cacopardi, G. Picardi, R. Sue, G. Levrini, and R. Perfetti, "Tracking algorithms in radars altimetry," in *Proc. Int. Geosci. Remote Sens. Symp., Remote Sens., Moving Toward 21st Century*, 1988, pp. 973–976.

[15] J. L. Whitten and B. A. Campbell, "Lateral continuity of layering in the Mars south polar layered deposits from SHARAD sounding data," *J. Geophys. Res., Planets*, vol. 123, no. 6, pp. 1541–1554, Jun. 2018.

[16] D. M. H. Baker and L. M. Carter, "Probing supraglacial debris on Mars 1: Sources, thickness, and stratigraphy," *Icarus*, vol. 319, pp. 745–769, Feb. 2019.

[17] G. A. Morgan et al., "Availability of subsurface water-ice resources in the northern mid-latitudes of Mars," *Nature Astron.*, vol. 5, pp. 230–236, Feb. 2021.

[18] L. Bruzzone et al., "RIME: Radar for icy moon exploration," in *Proc. IEEE Int. Geosci. Remote Sens. Symp. (IGARSS)*, Jul. 2013, pp. 3907–3910.

[19] D. D. Blankenship, D. A. Young, W. B. Moore, and J. C. Moore, "*Radar Sounding of Europa's Subsurface Properties and Processes: The View From Earth*. Tucson, AZ, USA: Europa. Univ. Arizona Press, 2009.

[20] M. C. Raguso, M. Mastrogiuseppe, R. Seu, and L. Piazzo, "Super resolution and interferences suppression technique applied to SHARAD data," in *Proc. 5th IEEE Int. Workshop Metrol. Aerosp. (MetroAeroSpace)*, Jun. 2018, pp. 242–246.

[21] R. Ghosh and F. Bovolo, "A hybrid CNN-transformer architecture for semantic segmentation of radar sounder data," in *Proc. IEEE Int. Geosci. Remote Sens. Symp.*, Jul. 2022, pp. 1320–1323.